

# Bistatic Experiment Using TerraSAR-X and DLR's new F-SAR System

S. V. Baumgartner, M. Rodriguez-Cassola, A. Nottensteiner, R. Horn, R. Scheiber, M. Schwerdt, U. Steinbrecher, R. Metzger, M. Limbach, J. Mittermayer, G. Krieger, A. Moreira  
Microwaves and Radar Institute, German Aerospace Center (DLR)  
Muenchner Strasse 20, 82234 Wessling, GERMANY, Email: stefan.baumgartner@dlr.de

## Abstract

A bistatic X-band experiment was successfully performed early November 2007. TerraSAR-X was used as transmitter and DLR's new airborne radar system F-SAR, which was programmed to acquire data in a quasi-continuous mode to avoid echo window synchronization issues, was used as bistatic receiver. Precise phase and time referencing between both systems, which is essential for obtaining high resolution SAR images, was derived during the bistatic processing. Hardware setup and performance analyses of the bistatic configuration are presented together with first processing results that verify the predicted synchronization and imaging performance.

## 1 Introduction

Bistatic radar techniques nowadays become more and more important for the remote sensing community since additional information can be gained in contrast to common monostatic radar techniques. The bistatic spaceborne-airborne X-band experiment has been carried out during the TerraSAR-X (TSX) commissioning phase for obtaining additional information about the TSX transmit channel by using F-SAR as an independent receiver. On the other hand, the experiment is an important preparation step for the TanDEM-X mission [2], since it enables e.g. the investigation of "in orbit" phase noise by exploiting transponder responses and since it also allows the performance verification of bistatic processing and imaging techniques.

A few years ago the Microwaves and Radar Institute of DLR and ONERA, the French Aerospace Lab, have performed successfully bistatic airborne X-band experiments using DLR's E-SAR and ONERA's RAMSES system [1]. Several bistatic configurations have been flown and both institutions have gained a lot of expertise in bistatic acquisitions. Nevertheless, to the authors' knowledge, no civilian bistatic X-band experiment between a SAR satellite and an airborne SAR system has been performed so far. Clock synchronization and drift compensation is essential for high-resolution bistatic SAR imaging. No information of frequency differences between both local oscillators is generally available, since they are spatially separated. For relaxing echo window synchronization requirements, F-SAR [3] is operated in a quasi-continuous receive-only mode. For the upcoming TanDEM-X mission special synchronization links, already installed on TSX, are foreseen [2]. Results of the bistatic campaign verified the feasibility of high-resolution bistatic imaging.

## 2 Bistatic Configuration

As test site for the bistatic experiment the calibration site of the Microwaves and Radar Institute located at the former military airfield in Kaufbeuren, Germany, was chosen. This test site has the advantage that the surrounding terrain is very flat. Hence, no additional processing problems due to terrain altitude changes are expected. For the bistatic experiment a left-looking backward scattering configuration as depicted in Fig. 1 was chosen. The on ground projected flight tracks of F-SAR and TSX are nearly parallel.

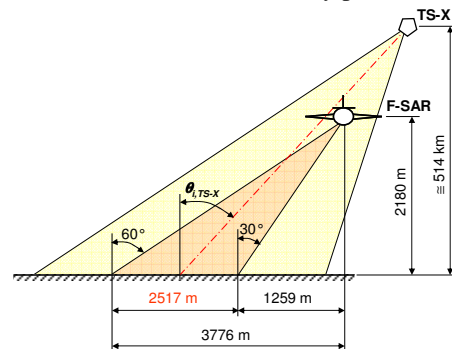


**Figure 1** Backward scattering configuration (not drawn to scale).

The incidence angle of TSX at scene center is  $\theta_{i,TS-X} = 55.63^\circ$  and the minimum range distance is 848.6 km. Due to the different platform velocities of F-SAR ( $\cong 90$  m/s) and TSX ( $\cong 7408$  m/s on-ground) the size of the imaged scene is mainly determined by the F-SAR antenna pattern (incidence angle range from  $30$  to  $60^\circ$ , azimuth 3 dB beamwidth  $8^\circ$ ). For an altitude of F-SAR of 2180 m above ground, the scene size is 2500 m in ground range. The azimuth extension varies with the incident angle and is approx. 350 m in near range and 600 m in far range.

### 3 System Setup

During the bistatic experiment F-SAR and TSX are operated with the same radar center frequency of 9.65 GHz. Since footprint overlapping occurs for only a few seconds, no significant relative oscillator drift is expected during the bistatic acquisition.

#### 3.1 F-SAR Configuration

To enable the new quasi-continuous receive-only mode with F-SAR, data acquisition has to be done by using two analog-to-digital converters (ADCs). The ADCs in F-SAR have a maximum sampling rate of 1 GS/s and a maximum duty cycle of 50 %. Thus, the ADCs cannot sample continuously. Hence, by using two ADCs and toggling between them with the clock of the system PRF, a quasi-continuous receiving mode becomes feasible. Due to data rate limitations only a reduced sampling rate of 250 MS/s can be used. Although the configuration sketched on the left of Fig. 2 is preferable due to SNR and processing aspects, the non-ideal configuration on the right is used since it can be realized with less effort (the configuration shown on the left of Fig. 2 requires a reconfiguration of the F-SAR antenna matrix which was not achievable during the experiment preparation time).

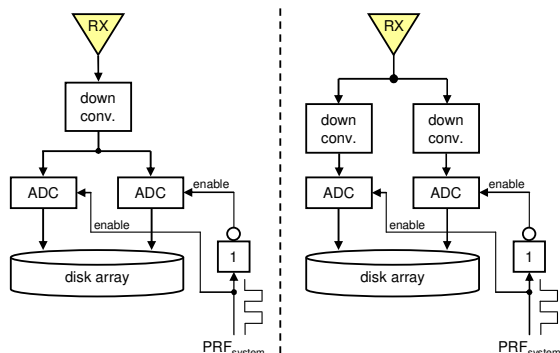


**Figure 2** Possible configurations for connecting two ADCs to a single receiving antenna in F-SAR.

To ensure an optimal recording level of the ADCs and to avoid clipping and saturation effects, the receiver gain in F-SAR has to be properly adjusted. Since the settling time of F-SAR’s automatic gain control system is in the order of the TSX illumination time of the scene, a fixed gain setting is used during the experiment. For a rough estimation of the expected power at the F-SAR antenna plug, it is sufficient to compare the power densities of both systems at the scene center. The power density difference is given as:

$$\Delta S = \frac{EIRP_{TS-X}}{4\pi r_i^2} - \frac{EIRP_{F-SAR}}{4\pi r_i^2}, \quad (1)$$

where  $EIRP_i$  is the effective radiated power of TSX and F-SAR and  $r_i$  is the distance to the bistatic scene center. For the proposed bistatic configuration the power density difference at scene center is  $\Delta S \cong -22$  dBm/m<sup>2</sup>. Thus, under the assumption that the scene

reflectivity remains the same for monostatic and bistatic data acquisition, F-SAR receiver gain has to be increased by 22 dB in contrast to monostatic operation (the 22 dB additional gain has been verified during the experiment with an accuracy of 3 dB).

#### 3.2 TerraSAR-X Configuration

For simplifying bistatic processing (i.e. the alignment of the echo windows) TSX is operated with a high PRF of 5921 Hz. Due to the limited sampling rate of 250 MS/s in F-SAR, the nominal range chirp bandwidth of TSX, which is 150 MHz, has to be reduced to values below 125 MHz (note that in F-SAR the real signal is sampled by the ADCs, I/Q demodulation is done afterwards by software). A range bandwidth of 100 MHz is used for the present experiment. For increasing the overlapping time of both antenna beams and thus improving the azimuth resolution, the high resolution spotlight mode of TSX is used. The decision to operate the satellite in the left-looking mode was made for avoiding conflicts with other calibration data takes planned over Germany.

### 4 Reference Targets on Ground

For evaluating the quality of the bistatic image and improving the processing accuracy some reference targets on ground are necessary. Although a field of corner reflectors is installed on the Kaufbeuren airfield, the bistatic beam width of the installed reflectors is below two degrees and thus, they might not be visible in the bistatic image. For this reason we have decided to use three X-band transponders as reference targets. Each of these transponders has a 3dB beamwidth of  $\geq 14^\circ$ . F-SAR has to be at a specified GPS waypoint broadside to the transponders with an absolute time accuracy of about  $\pm 5$  s to ensure that at least one transponder will be imaged. The EIRP of each transponder is set such that the power received by F-SAR from the transponder is in the same order as the total power received from the scene (cf. section 3.1).

### 5 Performance analysis

Since the proposed configuration is azimuth variant, conventional analysis of expected image resolution and SNR no longer holds. Several approximations must be made to account for the synthetic aperture essential to SAR image formation. The following values are computed using only the 3 dB apertures of the antennas, a flat Earth model and a maximum footprint overlapping time of 2.77 s. The used system parameters are listed in Table 1. For the center echo and the assumption that there is no along-track offset between both platforms, the range resolution is given as [4]:

$$\Delta r = \frac{c}{B_r} \cdot \frac{1}{\|\nabla r(x, y)\|} = \frac{c}{B_r} \cdot \frac{1}{\sin \theta_{TX} + \sin \theta_{RX}}, \quad (2)$$

where  $\theta_{TX}$  and  $\theta_{RX}$  are the incidence angles. Fig. 3 shows the resolution contours projected on ground. The image swath is cropped to a square region of  $3000 \times 400 \text{ m}^2$  around the  $45^\circ$  pointing of the F-SAR antenna. The resolution varies between 1.7 and 2.2 m. Due to the contribution of the shallow and almost constant incidence angle of TSX, on-ground range resolution of near range targets is better than in the purely monostatic airborne scenario.

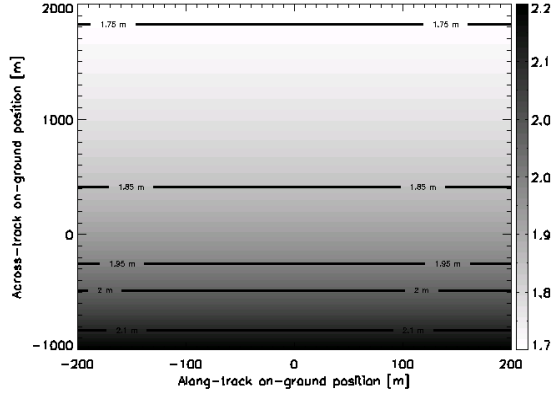


**Figure 3** Expected across-track resolution on ground.

Unlike more usual SAR configurations, azimuth bandwidth is mainly defined by satellite motion, whereas along-track resolution is dominated by the airborne contribution. Assuming a linear model for the instantaneous Doppler frequency of scene targets within the joint beam, along-track resolution can be computed using the results presented in [4] as:

$$\Delta x = \frac{1}{T_{int}} \cdot \frac{1}{\|\nabla f_{Dop}(x, y)\|} = \frac{\lambda}{T_{int}} \left( \frac{v_{TX}}{r_{TX}} + \frac{v_{RX}}{r_{RX}} \right)^{-1}, \quad (3)$$

where  $f_{Dop}$  is the Doppler frequency and  $T_{int}$  is the integration time. The along-track resolution map for this bistatic configuration is shown in Fig. 4.

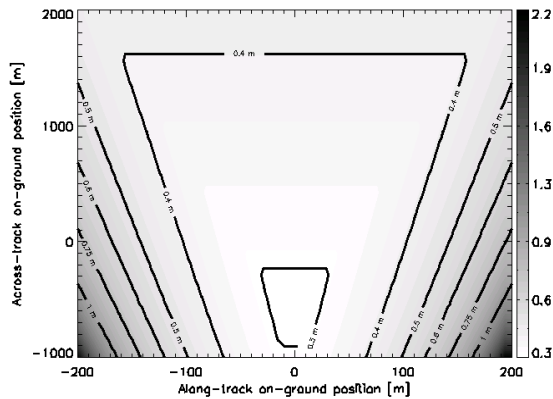


**Figure 4** Expected along-track resolution.

Due to the spotlight character of the acquisition, integration times  $T_{int}$  for targets placed on the center of the image are higher than for targets on the edges; the best attainable resolution approaches 0.3 m and decreases with  $T_{int}$  around the edges of the scene to 2.2 m. The monostatic TSX along-track resolution for the selected scene is more or less constant and approaching

0.65 m. The sensitivity of the system is measured by the bistatic noise-equivalent-sigma-zero (NESZ). The NESZ is computed using the formula presented in [4]:

$$NESZ = \frac{(4\pi)^2 r_{TX}^2 r_{RX}^2 k T_s F L}{P_i G_{TX} A_{RX} A_{rescell} T_{int}}, \quad (4)$$

where  $A_{rescell}$  is the resolution cell area on ground obtained from the previous bistatic across-track and along-track resolution maps. NESZ takes an approximate value of -40 dB in scene center. Typical NESZ values for the monostatic TSX acquisition are around -20 dB, due to the longer two-way range for the satellite case.

**Table 1** System parameters.

Speed of light	$c$	$2.9979 \cdot 10^8 \text{ m/s}$
Boltzmann's constant	$k$	$1.38 \cdot 10^{-23} \text{ Ws/K}$
Wavelength	$\lambda$	3.1 cm
Range bandwidth	$B_r$	100 MHz
Average transmit power	$P_i$	370 W
Antenna gain TX	$G_{TX}$	46.35 dBi
Antenna size TX	$A_{TX}$	$0.7 \times 4.784 \text{ m}^2$
Antenna size RX	$A_{RX}$	$0.046 \times 0.2 \text{ m}^2$
Velocity of F-SAR	$v_{RX}$	90 m/s
Velocity of TSX	$v_{TX}$	7408 m/s
Altitude of F-SAR	$h_{F-SAR}$	2180 m
Altitude of TSX	$h_{TS-X}$	514 km
Noise figure + losses	$F+L$	4.5 dB
Receiver noise temperature	$T_s$	300 K

## 6 Experimental Results

Both monostatic and bistatic data have been processed, confirming the expected results obtained in the previous section. Synchronization of the bistatic raw data was performed with an accuracy of 0.5 Hz by using the direct signal and a transponder on ground. Due to the use of two different down-converter paths during the acquisition (cf. Fig. 2, right), channel equalization has been shown to be essential to avoid non-linear modulations in the bistatic data set. Because of the strongly non-stationary character of the acquisition and the high resolution values, bistatic data have been processed using a bistatic extension of the backprojection algorithm. Fig. 7 shows the focused bistatic image projected on an on-ground grid and Fig. 8 shows a detail of the monostatic high resolution spotlight TSX image (left) and the corresponding bistatic image (right). As it was expected, the monostatic image has a poor performance in terms of range ambiguities due to the large off-nadir angle and the high PRF selected for the acquisition. Along-track resolutions for both images are 0.65 m and 0.35 m in scene center, respectively. Fig. 6 shows the along-track responses of the center transponder for ideal bistatic (black), actual bistatic (red) and monostatic (blue) acquisitions. Defocusing in the bistatic case is due to residual phase errors caused mainly by the motion of the airborne

platform. Nevertheless, the resolution shows a similar value (0.35 m) as the ideal bistatic response.

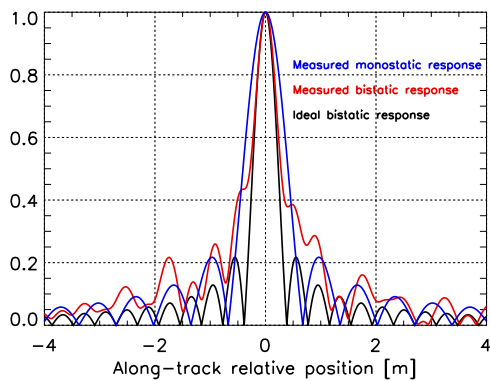


**Figure 6** Ideal and measured impulse responses.

## 7 Conclusions

The bistatic experiment between TSX and F-SAR has been conducted successfully. Synchronization of bistatic data set was shown to be possible in processing stages. The bistatic image also shows a better resolution in the scene center, a higher SNR and no range ambiguities, as it was expected from the performance analysis.

## Acknowledgement

The authors would like to thank their colleagues Jens Fischer and Christian Andres for pre-processing the F-SAR data and Nuria Tous, Adriano Meta, Carlos Ortega and Marwan Younis for fruitful discussions regarding processing of TSX data and performance.

## References

- [1] M. Wendler, G. Krieger, R. Horn, B. Gabler, P. Dubois-Fernandez, B. Vaizan, O. Du Plessis, H. Cantalloube, "Results of a Bistatic Airborne SAR Experiment," Proceedings of IRS 2003, Dresden, Germany, September 2003.
- [2] G. Krieger and M. Younis, "Impact of Oscillator Noise in Bistatic and Multistatic SAR," IEEE Geoscience and Remote Sensing Letters, Letters, vol. 3, no 3, July 2006, pp. 424-428.
- [3] R. Horn, A. Nottensteiner and R. Scheiber, "F-SAR – DLR's advanced airborne SAR system onboard DO228," Proceedings of EUSAR 2008, Friedrichshafen, Germany, June 2008.
- [4] G. Krieger, H. Fiedler, D. Hounam and A. Moreira, "Analysis of System Concepts for Bi- and Multi-Static SAR Missions," Proceeding of IGARSS 2003, Toulouse, France, July 2003.



**Figure 7** Bistatic X-band image of the test site Kaufbeuren (horizontal axis: range, vertical axis: azimuth).

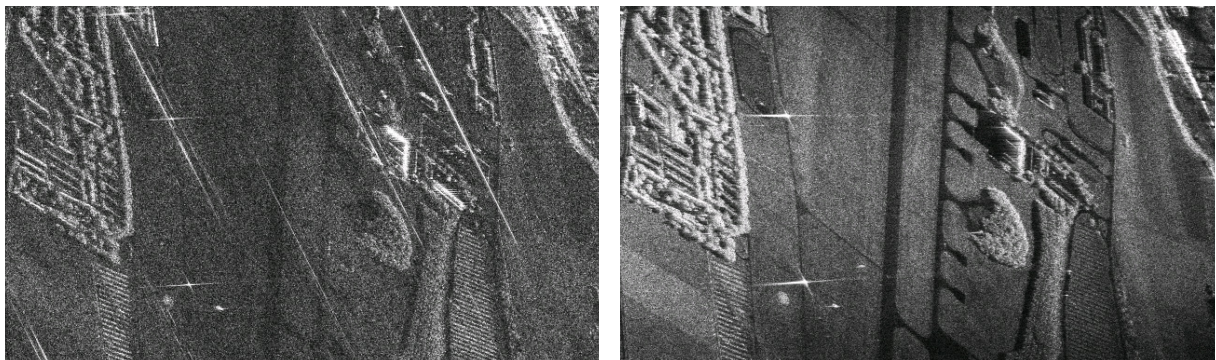


**Figure 8** Detail of monostatic TSX image (left) and bistatic image (right) showing the airfield and two transponders. Note: TSX acquisition parameters have been modified for the bistatic experiment and are thus improper for monostatic TSX acquisition (e.g. occurrence of range ambiguities due to high PRF and shallow inc. angle).